Article

Drug Permeability Assay Using Microhole-Trapped Cells in a Microfluidic Device

Ju Hun Yeon, and Je-Kyun Park

Anal. Chem., **2009**, 81 (5), 1944-1951• DOI: 10.1021/ac802351w • Publication Date (Web): 09 February 2009

Anal. Chem. **2009,** *81,* 1944–1951

Drug Permeability Assay Using Microhole-Trapped Cells in a Microfluidic Device

Ju Hun Yeon and Je-Kyun Park*

Department of Bio and Brain Engineering, College of Life Science and Bioengineering, KAIST, 335 Gwahangno, Yuseong-gu, Daejeon 305-701, Republic of Korea

As orally administered drugs must be absorbed from the intestine into the blood circulation, permeability assays of drug candidates have been widely used in the early screening stages of drug discovery. In this study, a microfluidic device was developed for the drug permeability assay, considering the in vivo delivery path of drugs in humans. A microhole array for cell trapping was fabricated using the poly(dimethylsiloxane) (PDMS) molding technique by mimicking the intestinal epithelial cell membrane. On the basis of mathematical simulations, the configuration of the microfluidic device, including a microhole array and a mixing channel, was optimized to trap cells firmly in each microhole. At the flow rate under optimal conditions, cells were effectively trapped in a microhole array without cell damage. We measured the permeability of 10 drugs, including those with high and low permeability in microchannels, and compared the results with the reported values of permeability in the human and rat intestine. Most drugs had a high *p* value ($p > 0.4$), and only a few drugs had a low *p* value less than 0.05 by *t* test. Though their measured permeabilities are not the same as those in vivo human intestine, it shows that in vivo permeabilities in the human and rat intestine are highly correlated with those measured by the microfluidic device ($R^2 = 0.9013$ and $R^2 = 0.8765$, respectively). Also, the fraction of the dose absorbed in the human intestine (F_a) indicated that the drug permeability measured using this device was significantly correlated ($R^2 = 0.9641$) with those in human subjects. As the microfluidic assay system is dependent on cells trapped inside a microhole array, it is a valuable tool in drug discovery as well as an alternative to animal testing.

Drugs are generally administered via the oral route. As orally administered drugs must be absorbed from the intestine into the blood circulation, the selection of drug candidates with high oral absorption potential based on a permeability assay is one of the most important steps in drug discovery. Consequently, a rapid and accurate method for measuring drug permeability in the human intestine is a priority for the pharmaceutical industry.[1−5] As studying and measuring the intestinal permeability in the human body or replacing animal testing is difficult, many alternative in vitro or in situ assay methods have been developed to investigate the intestinal absorptive potential and absorption mechanisms of drugs.

For an in vitro permeability assay, a method based on monolayers of the human colon adenocarcinoma endothelial cell line Caco-2 has been widely used due to the remarkable morphological and biochemical similarities of the Caco-2 cell membrane to that of small intestinal epithelium cells.[6,7] Despite the similarities, however, the limitations of this method include the long culture period of Caco-2 cells and the occasional inconsistency with in vivo permeability. To overcome the former problem, 3−10 day Caco-2 procedures or the fast growing Madin−Darby canine kidney (MDCK) cell line have been developed, but the 3 day culture method requires expensive media for fast differentiation. As 80−95% of commercial drugs are absorbed primarily by passive diffusion, the parallel artificial membrane permeability assay (PAMPA)[2,8,9] and immobilized artificial membrane (IAM)[3,10] were developed for rapid and inexpensive assays dealing solely with passive diffusion. PAMPA uses lipid oils mimicking the lipid bilayer of cellular membranes and measures drugs passively diffusing through the lipid layer. The lipid layer of PAMPA replaces the cultured cells and therefore makes it possible to measure the drug permeability instantly. However, due to the lack of transport proteins of intestinal cells in the lipid layer of PAMPA, it could be implemented only for hydrophobic drugs absorbed passively. IAM, the surface of which contains one-half of the membrane bilayer, is another approach for measuring permeability because it has a good correlation with transport of drugs across Caco-2 cells. However, it is not predictive across classes of

* To whom correspondence should be addressed. E-mail: jekyun@kaist.ac.kr. Phone: +82-42-350-4315. Fax: +82-42-350-4310.

(1) Zakeri-Milani, P.; Valizadeh, H.; Tajerzadeh, H.; Azarmi, Y.; Islambolchilar, Z.; Barzegar, S.; Barzegar-Jalali, M. *J. Pharm. Pharmceut. Sci.* **2007**, *10*, 368–379.
(2) Balimane, P. V.; Han, Y.-H.; Chong, S. *AAPS J.* **2006**, *8* (1), E1–E13.
(3) Bohets, H.; Annaert, P.; Mannens, G.; van Beijsterveldt, L.; Anciaux, K.; Verboven, P.; Meuldermans, W.; Lavrijsen, K. *Curr. Top. Med. Chem.* **2001**, *1*, 367–383.
(4) Caldwell, G. W.; Ritchie, D. M.; Masucci, J. A.; Hageman, W.; Yan, Z. *Curr. Top. Med. Chem.* **2001**, *1*, 353–366.
(5) Shearer, T. W.; Smith, K. S.; Diaz, D.; Asher, C.; Ramirez, J. *Comb. Chem. High Throughput Screening* **2005**, *8*, 89–98.
(6) Wang, Z.; Hop, C.; Leung, K. H.; Pang, J. *J. Mass Spectrom.* **2000**, *35*, 71–76.
(7) Hubatsch, I.; Ragnarsson, E.; Artursson, P. *Nat. Protoc.* **2007**, *2*, 2111–2119.
(8) Kerns, E. H.; Di, L.; Petusky, S.; Farris, M.; Ley, R.; Jupp, P. *J. Pharm. Sci.* **2004**, *93*, 1440–1453.
(9) Ottaviani, G.; Martel, S.; Carrupt, P.-A. *J. Med. Chem.* **2006**, *49*, 3948–3954.
(10) Chan, E. C. Y.; Tan, W. L.; Ho, P. C.; Fang, L. J. *J. Chromatogr.* **2005**, *1072*, 159–168.

10.1021/ac802351w CCC: $40.75
Published on Web 02/09/2009

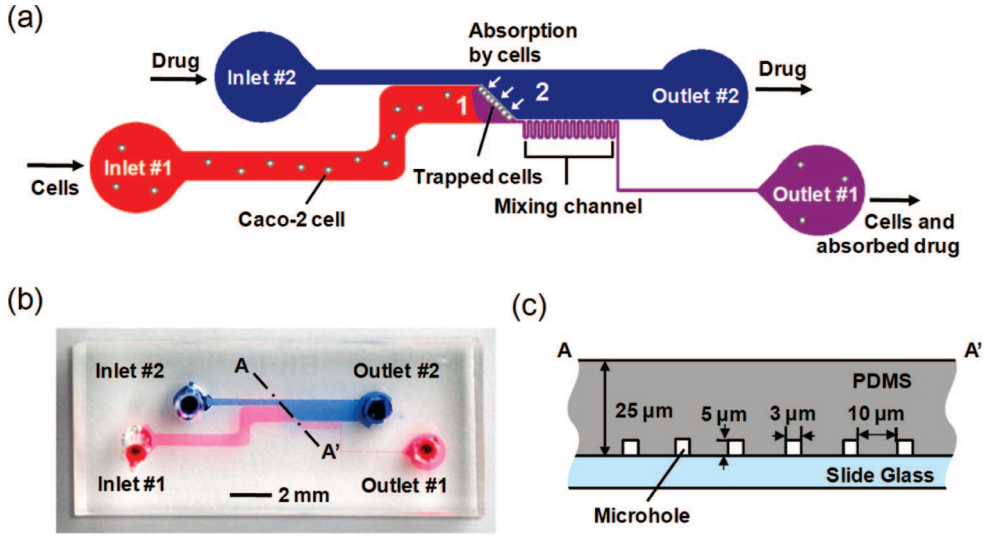

Figure 1. Schematic diagrams and photograph of the microfluidic device. (a) The drug absorption and transport process on the microfluidic device. Caco-2 cells resuspended in culture media are injected into inlet no. 1 (red flow) and trapped in the microhole array. Then, drugs are injected into inlet no. 2 (blue flow) and absorbed by the trapped cells through the holes (violet flow). Exactly, the drug is absorbed by trapped cells from region 2 to region 1 (indicated by small white arrows). (b) A photograph of the fabricated device for drug permeability assay. (c) A schematic side view of the A−A′ cross section showing the microhole array for cell trapping in detail.

compounds because its membrane based on lipophilicity and electrostatic interaction may only be valid for compounds with similar structures.

As an in situ permeability assay, the single-pass intestinal perfusion (SPIP) approach is frequently used to provide a preserved microenvironment above the intestinal membrane because drugs are absorbed across the real intestinal cell barriers and encounter the blood circulation, resulting in a good correlation with the in vivo behavior in humans.[1,3,11−14] Despite accurate measurement, however, this technique requires skilled operators, due to the involvement of a surgical method in rats, and significant investment in terms of resources to set up, validate, and run. In addition, the use of anesthetics may have an influence on the membrane permeability, cellular metabolism, and lack of certain nutrients or other endogenous compounds.

Recently, microfluidic technology has been introduced in the fields of cellular assay and drug discovery because it can provide an in vivo-like microenvironment, continuous perfusion, and high-throughput screening.[15,16] For example, the microfluidic system for long-term perfusion culture was applied to Caco-2 cells for 2 weeks, and then the transport of rhodamine 123 was monitored.[16] However, performing permeability assays using real drugs is necessary. Genes et al.[17] presented a vascular endothelium array with blood components using microfluidic channels, and Suzuki et al.[18] developed a planar lipid bilayer in a microfluidic device for studying membrane proteins. These studies indicated that high-throughput drug discovery would be possible using a multiarray system and lipid-bilayer structure, but it still requires complex fabrication processes and has not been used to continuously measure the permeability of real drugs.

In the present study, we developed a permeability assay system using a microfluidic device inspired by the in vivo drug absorption mechanisms in the intestine. The device structure and experimental conditions were optimized through mathematical simulations and verified experimentally. The permeabilities of 10 well-known drugs were then measured using our device, and the results were compared with their in vivo permeabilities.

EXPERIMENTAL SECTION

Design of a Microfluidic Device for Drug Permeability Assays. We designed a new microfluidic permeability assay system based on absorption mechanisms in the intestine. Conventional permeability assay systems require embedded membrane structures for culturing epithelial cells or mimicking the cell membrane. Instead of a membrane structure, we used microholes for trapping Caco-2 cells and measured the permeabilities of drugs absorbed through the trapped Caco-2 cells without long-term cell culture. The microfluidic device includes two inlet parts, two outlet parts, a microhole array for cell trapping, and a mixing channel. As shown in Figure 1, parts a and b, Caco-2 cells from inlet no. 1 are supplied to outlet no. 1 at a flow rate of 20 μL/h while fresh buffer from inlet no. 2 is supplied to outlet no. 2 at a flow rate of 20 μL/h. Due to the difference of pressure in the holes, the injected cells are automatically trapped in the microhole array. After the cell trapping, fresh medium without any cells from inlet no. 1 is constantly supplied to outlet no. 1 and a fluorescent dye or drug solution to be assayed is injected into inlet no. 2. The dye or drug is then absorbed by the trapped cells and transported to region 1 from region 2 of the channel, and then to the mixing channel connected to outlet no. 1. We introduce the mixing channel to uniformly distribute the absorbed

(11) Stretch, G. L.; Nation, R. L.; Evans, A. M.; Milne, R. W. *Drug Dev. Res.* **1999**, *46*, 292–301.
(12) Song, N.-N.; Li, Q. S.; Liu, C. X. *World J. Gastroenterol.* **2006**, *12*, 4064–4070.
(13) Winne, D. *Naunyn-Schmiedeberg's Arch. Pharmacol.* **1979**, *307*, 265–274.
(14) Zakeri-Milani, P.; Barzegar-Jalali, M.; Tajerzadeh, H.; Azarmi, Y.; Valizadeh, H. *J. Pharm. Biomed. Anal.* **2005**, *39*, 624–630.
(15) Yeon, J. H.; Park, J.-K. *BioChip J.* **2007**, *1*, 17–27.
(16) Kimura, H.; Yamamoto, T.; Sakai, H.; Sakai, Y.; Fujii, T. *Lab Chip* **2008**, *8*, 741–746.
(17) Genes, L. I.; Tolan, N. V.; Hulvey, M. K.; Martin, R. S.; Spence, D. M. *Lab Chip* **2007**, *7*, 1256–1259.
(18) Suzuki, H.; Tabata, K.; Kato-Yamada, Y.; Noji, H.; Takeuchi, S. *Lab Chip* **2004**, *4*, 502–505.

dye or drug because the transported chemicals are not uniformly diffused in the microchannel due to laminar flow. The concentrations of drugs are monitored in outlet no. 1.

A schematic side view of cross section A−A′ in Figure 1b shows the size of microhole in the microhole array (Figure 1c). Because the diameter of Caco-2 cells is about 10 μm, we determined the width of the microhole to 3 μm and the height of the microhole to 5 μm for trapping cells firmly in the microholes. The distance between microholes was determined by the cell size of 10 μm for constituting a tightly compacted cell monolayer in a microhole array. The length of the microhole is 30 μm for minimizing the cell lysis by fluid flow. The microchannel height is 25 μm for freely moving cells in a microfluidic device. Therefore, most animal cells with the diameter of 5−15 μm could be trapped on the microholes of this device. The overall size of the microfluidic device is 19 mm × 8 mm as shown in Figure 1b.

Microfabrication Process. The microfluidic device for drug permeability assays was fabricated using a multilayer lithography method. First, the design pattern for a microfluidic channel was printed onto a Cr mask. The mold master for devices was fabricated using a negative photoresist (PR) (SU-8 2005; Microlithography Chemical Co., Newton, MA) to manufacture a microhole array with conventional lithography. The second negative PR (SU-8 2025; Microlithography Chemical Co.) was coated and exposed after aligning with the align mark of the first layer. After the second development, the prepolymer of poly(dimethylsiloxane) (PDMS) (Sylgard 184; Dow Corning, Midland, MI) was mixed with a curing agent at a 10:1 mass ratio and poured over the mold masters. Then, the PDMS structure was cured at 65 °C for 1 h and peeled from the mold.

Cell Culture. The human colon adenocarcinoma endothelial cell line Caco-2 (ATCC HTB37) was selected for the microfluidic drug permeability assay. Cell layers cultured on Petri dishes were rinsed briefly with phosphate-buffered saline (PBS) with a pH of 7.4 (Gibco, Grand Island, NY). Then, trypsin−EDTA solution (0.25% trypsin and 1 mM EDTA·4Na; Gibco) was used to detach the cells and modified Eagle's medium (MEM; Gibco-BRL, Gaithersburg, MD) supplemented with 20% fetal bovine serum (FBS; Gibco) was added to the dispersed cell layer. The cell cultures were maintained at 37 °C under 5% CO_2 in a humidified water-jacketed incubator.[19] Prior to the permeability assay using the microfluidic device, appropriate aliquots of the cell suspension were refreshed and diluted to a suitable concentration of 2.5×10^6 cells/mL. Drug-treated cells and reagents after the experiments were completely autoclaved before discharging to ensure safety according to the KAIST experimental protocols for biosafety.

Experimental Setup. The microfluidic devices were sterilized, and the bubbles within the channel were eliminated with 70% ethanol for 10 min, followed by rinsing with cell culture media. Caco-2 cells were incubated in the culture dishes, and then 100 μL of 1×10^7 cells/mL was injected into inlet no. 1 of the microfluidic device and 100 μL of drugs or fluorescein isothiocyanate (FITC)−dextran (Sigma-Aldrich, Seoul, Korea) was also injected into inlet no. 2. The concentration of fluorescent dye was estimated by measuring the fluorescence intensity of reference samples in the mixing channel.

Computational Fluid Dynamics Simulation. Simulations of the fluid flow in the slanted microhole array structures were performed with commercial software (CFD-ACE+; ESI, Huntsville, AL). The microhole for simulation is 3 μm in width, 5 μm in height, and 30 μm in length (Figure 1c). The number of microholes is one half of the real microfluidic device. Upwind scheme was used in the conjugates gradient squared (CGS) and preconditioning (Pre) solvers for the velocity field, whereas algebraic multigrid (AMG) solver was used for pressure correction. The inlet fluid velocity was varied, and the boundary conditions at the outlet were set at a fixed pressure. Water was used as a test sample.

HPLC Analysis. All drugs, including propranolol, naproxen, furosemide, antipyrine, verapamil, atenolol, piroxicam, hydrochlorothiazide, cimetidine, and carbamazepine, were purchased from Sigma-Aldrich. Other chemicals or reagents were purchased from Merck (Seoul, Korea). For drugs, a solution obtained for 2 h from outlet no. 1 was analyzed by reversed-phase high-performance liquid chromatography (HPLC) (Agilent 1100 series; Agilent Technologies, Santa Clara, CA) with an Eclipse Plus C18 (5 μm, 4.6 mm × 250 mm) column (Agilent Technologies). For HPLC analysis, 5 μL aliquots of the samples were applied and buffers were passed through the column at a rate of 1 mL/min under isocratic conditions. The mobile phases were filtered through 0.46 μm sintered glass filters (Millipore, Bedford, MA) and degassed in a sonicator (Branson, Danbury, CT) before use. Each drug concentration was estimated from the drug reference samples.

Data Analysis. The effective permeability coefficient (P_{eff}) was derived from eq 1, the conventional equation of the steady-state condition for adapting a microfluidic perfusion system[7,20]

$$P_{\mathrm{eff}} = \frac{1}{AC_0}\frac{\mathrm{d}Q}{\mathrm{d}t} \tag{1}$$

where P_{eff} is the permeability (cm/s), A is the surface area (cm^2), C_0 is the initial concentration (mM), and Q is the number of absorbed molecules (mol). In our device, the surface area (A) is determined by multiplying the hole number in the microhole array (76 trapping holes) by each hole area (1.5×10^{-7} cm^2). Here, eq 2 is an integrated form of eq 1 for time Δt

$$Q(t) = P_{\mathrm{eff}} A C_0 \Delta t \tag{2}$$

As the flow rate of inlet no. 1 is v (cm^3/s), the volume flowing in channel no. 1 for Δt is $v\Delta t$. The concentration of molecules transported from channel region 2 to channel region 1 for time Δt is expressed by eq 3:

$$C = \frac{Q(t)}{v\Delta t} = \frac{P_{\mathrm{eff}} A C_0}{v} \tag{3}$$

From eq 3, we derived the effective permeability equation (eq 4) where $v = 10$ cm^3/s and $A = 1.2 \times 10^{-5}$ cm^2. The initial concentration C_0 for each drug was determined from the literature:

$$P_{\mathrm{eff}} = v\frac{C}{C_0}\frac{1}{A} \tag{4}$$

(19) Yeon, J. H.; Park, J.-K. *Anal. Biochem.* **2005**, *341*, 308–315.

(20) Grassi, M.; Cadelli, G. *Int. J. Pharm.* **2001**, *229*, 95–105.

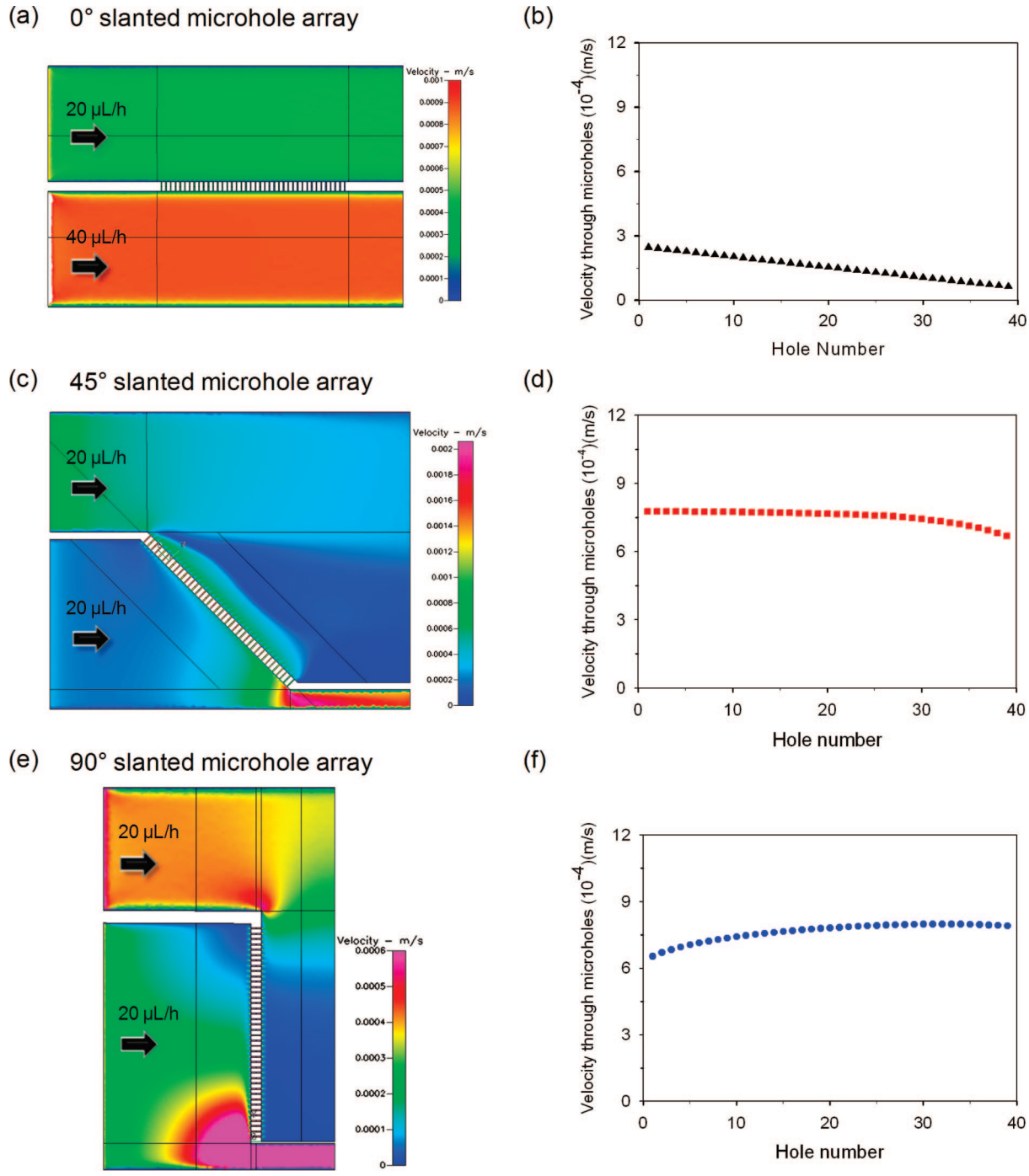

Figure 2. Simulation results to determine the optimal slanted angle and flow rates. The left figures stand for the calculated velocity profiles in each microchannel, whereas the right figures denote the velocity distribution according to the hole number in a microhole array. (a and b) For the 0° slanted microhole array, the flow rate crossing holes gradually decreased in the rearward holes. (c and d) For the 45° slanted microhole array, the flow rate crossing holes was constant over all holes. (e and f) The 90° slanted microhole array showed similar results of flow rate as in the 45° slanted structure.

RESULTS AND DISCUSSION

Simulation for Optimizing the Device Structure. We performed simulations to optimize the device structure for trapping cells, including the angle of the microhole array and the flow rates in both channels. The microhole array was tilted by 90°, 60°, 45°, 30°, or 0° along the horizontal axis. For the 0° slanted microhole array, the fluid flowed from the channel of high flow rate to that of low flow rate and the flow rate crossing holes decreased gradually in the rearward holes (Figure 2, parts a and b). Due to this decreased flow rate, the cells would not be trapped in these holes. For angles of 30° and 60°, the flow rate through the holes decreased slightly in the rearward holes. For the 45° slanted microhole array, the flow rate was constant over all holes (Figure 2, parts c and d). The 90° slanted microhole array showed similar phenomena as the 45° slanted structure (Figure 2, parts e and f). The simulation results indicated that the array structure slanted

at an angle of 45° produced the best conditions for cell trapping. The simulation results were also validated experimentally (data not shown). The experimental results for 30° and 60° slanted structures showed that the cells in the rearward holes were not trapped as predicted. Increasing the flow rate to trap cells in these holes resulted in lysis of the trapped cells. For the 90° slanted structure, cells were trapped over all holes, but cells piled up with an irregular thickness, which would result in different absorption rates in each hole. On the basis of the simulation and experimental results, the cell trapping structure slanted by 45° was selected for stable cell trapping to form a single layer of cell.

In addition, we optimized the flow rates in both channels to trap cells firmly, varying flow rates of 5, 10, and 20 μL/h in each inlet of a microchannel with the 45° slanted microhole array. The flow was monitored using FITC−dextran before and after the cell trapping. As the flow rate ratio of inlet no. 1 to inlet no. 2 increased, the velocities moving through holes gradually increased. The flow rate ratio of 1:1 resulted in the best results to produce similar flow velocities in each hole. The flow rates of 5 and 10 μL/h were too slow to trap cells, and cell debris was caught in the holes because of the faster movement of debris compared to that of cells. From this simulation and experimental results, we determined the flow rate as 20 μL/h in each inlet for stable cell trapping. After the cell trapping, to minimize the cell damage due to pressure at a high flow rate of 20 μL/h in the two inlets, we adjusted the flow rate to 10 μL/h in both channels, maintaining the flow rate constant over all trapping holes. The simulation results also show that the pressure difference between two channels was too small at a flow rate of 10 μL/h (data not shown). Therefore, we expect that the damage of trapped cells due to pressure would be minimized.

Permeability Assay with FITC−Dextran. To demonstrate the working principle of the microfluidic device using trapped cells in a microhole array, FITC−dextran was used to verify the absorption of drugs through the trapped cells. FITC−dextran is a widely used tracer in microcirculatory systems and in vitro or in vivo permeability studies because it is absorbed through epithelial cells and can be readily visualized under high-resolution fluorescence microscopy.[21,22] Caco-2 cells and FITC−dextran were injected into inlet no. 1 and inlet no. 2, respectively. FITC−dextran was absorbed and transported by the trapped Caco-2 cells, and the fluorescence intensity of FITC−dextran in the mixing channel was measured. The intensity of the absorbed FITC−dextran increased gradually over time and was saturated after 2 h as shown in Figure 3. If exceptional leakage occurred on the microhole, medium fluid flowed from region 1 to region 2 and the concentration of absorbed FITC−dextran in the mixing channel decreased (Figure 1 in the Supporting Information). Therefore, we could notice whether microholes have leakage or not. Whenever we perform experiments, we precisely controlled the flow rate for diminishing the leakage by the cell lysis.

Morphology of Trapped Cells and the Viability Test. During the assay, the lysis of trapped cells on the microhole array would reduce drug transport and also open holes causing drug leakage, consequently affecting the drug absorption rate. The key factors for controlling cell trapping are the flow rate and cell density in a microchannel. Therefore, it is possible to form single-layered cells or multilayered cells by controlling these factors. When cells with a density of 1×10^7 cells/mL were supplied at a flow rate of 20 μL/h, cells were trapped on the microhole array with a single layer. However, a higher cell density or slower flow rate frequently resulted in cell stacking on the microholes. In this study, we precisely controlled the flow rate and cell density to form a single layer throughout our experiments. At an optimal flow rates, cells were trapped in the microhole array and observed as shown in Figure 4a. From the magnified photograph of the trapping hole, it seems that Caco-2 cells closed the holes in a single layer. To ensure cells were viable during the assay, we observed the cell viability for 3 h using Hoechst 33342 and propidium iodide (PI), which stain the nuclei of viable and dead cells blue and red, respectively. As shown in Figure 4b, most cells were viable for 2 h and the effect of dead cells would be negligible, but the number of lysed cells increased after 3 h under the influence of fluid flow. As drug absorption was saturated within 2 h (Figure 3), we measured drug permeability within 2 h to exclude measurement errors caused by the dead cells. This device can also be used for forming multilayered structure of different cells in a microfluidic device if at least two types of cells are supplied for trapping purpose. However, more experimental studies including device modification are required for forming the multiple layers of different cells on the microhole array.

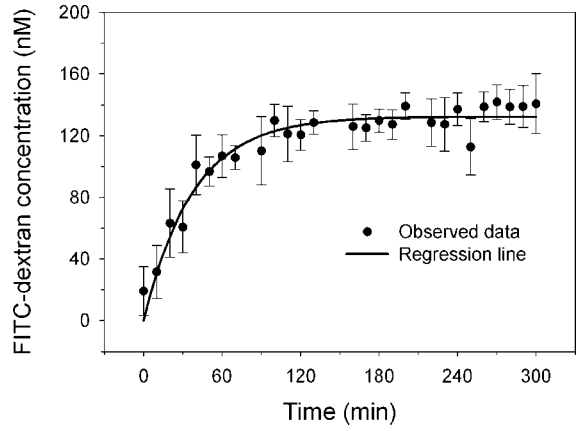

Figure 3. Fluorescence intensity of the absorbed FITC−dextran (n = 3). The intensity of absorbed FITC−dextran by the trapped Caco-2 cells increased gradually over time and became saturated after 2 h. The intensity of FITC−dextran in the mixing channel was measured under a fluorescence microscope.

Drug Permeability Assay. We analyzed 10 well-known drugs using our microfluidic device and compared the data to the in vivo findings in humans and rats reported in the literature. The selected drugs are commonly used as, for example, antihypolipidemic agents, antiulcer agents, or diuretics. A more reliable prediction of drug permeability would be obtained using a larger number of model drugs with a broad range of physicochemical properties, i.e., both high-permeability drugs, such as propranolol, naproxen, and antipyrine, and low-permeability drugs, such as cimetidine, atenolol, and furosemide. Ten drugs absorbed on the microfluidic device were analyzed by reversed-phase HPLC according to the reported experimental conditions.[1,10,13,23−27] The effective permeability, P_{eff} (cm/s), of drugs was calculated by

(21) Thorball, N. *Histochemistry* **1981**, *71*, 209–233.
(22) Olsson, Y.; Svensjö, E.; Arfors, K.-E.; Hultström, D. *Acta Neuropathol.* **1975**, *33*, 45–50.
(23) Kim, J.-S.; Mitchell, S.; Kijek, P.; Tsume, Y.; Hilfinger, J.; Amidon, G. L. *Mol. Pharm.* **2006**, *3*, 686–694.

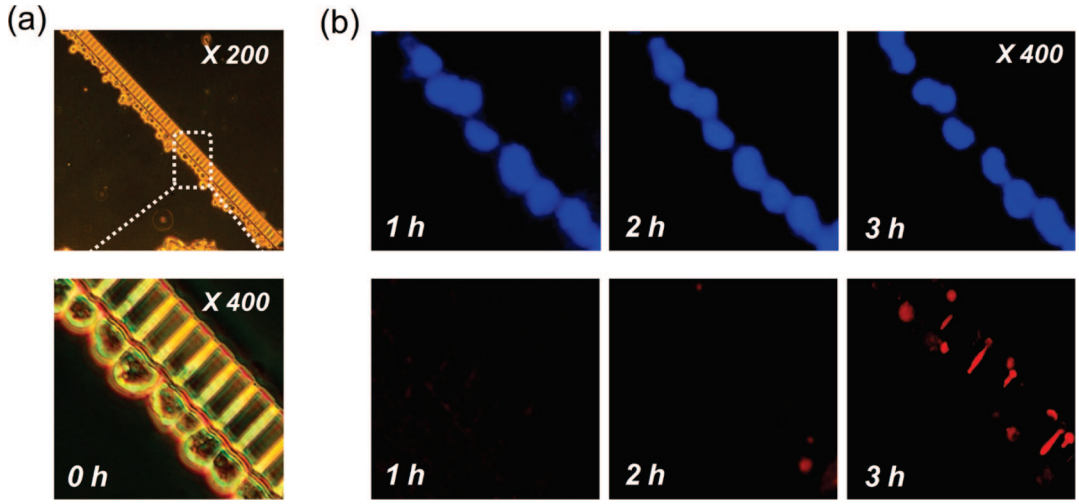

Figure 4. Trapped cell morphology and cell viability over time during the drug absorption assay. (a) The trapped cells on the microhole array in a single layer without lysis. (b) The Caco-2 cells trapped in the holes were stained with Hoechst 33342 and propidium iodide (PI). Viable cells were stained blue by Hoechst 33342 (upper row) and dead cells were stained red by PI (lower row).

Table 1. Effective Permeability (P_{eff}) on the Microfluidic Device, Human P_{eff}, Rat P_{eff}, and the Fraction of the Dose Absorbed in the Human Intestine (F_a) Values of Tested Drugs

compd	device P_{eff} (10^{-4}) (cm/s)	human P_{eff} (10^{-4}) (cm/s)	rat P_{eff} (10^{-5}) (cm/s)	F_a (%)
propranolol	3.9 ± 1.7	2.9 ± 1.3 (refs 23, 35)	5.6 ± 2.0 (ref 1)	100 (ref 23)
naproxen	10.9 ± 4.1	10.0 ± 4.7 (ref 36)	11.9 ± 1.2 (ref 23)	100 (ref 23)
furosemide	1.1 ± 0.3	0.3 ± 0.3 (ref 1)	3.3 ± 2.0 (ref 1)	61 (ref 23)
antipyrine	9.5	5.6 ± 1.6 (ref 36)	5.9 ± 0.2 (ref 1)	100 (ref 23)
verapamil	5.2 ± 0.1	6.70 ± 2.90 (ref 23)	6.5 ± 0.5 (ref 23)	100 (ref 23)
atenolol	0.6 ± 0.1	0.12 ± 0.20 (ref 36)	0.60 ± 0.60 (ref 23)	50 (ref 23)
piroxicam	8.0	6.7 (ref 1)	7.9 ± 4.0 (ref 1)	100 (ref 23)
hydrochlorothiazide	2.7 ± 1.6	0.04 ± 0.05 (ref 23)	2.0 ± 1.0 (ref 1)	67 (ref 23)
cimetidine	0.2	0.30 ± 0.05 (ref 23)	4.8 ± 0.1 (ref 1)	60 (ref 23)
carbamazepine	1.5	4.3 ± 2.7 (ref 23)	6.2 ± 0.6	97 (ref 1)

eq 4 and is shown in Table 1.[1,28–31] The in vivo permeabilities in the human and rat intestine showed correlations with those measured by the microfluidic device (R^2 = 0.9013 and R^2 = 0.8765, respectively). As shown in Figure 5, the permeability of each drug was plotted with a 95% prediction interval. In particular, the P_{eff} values measured on the microfluidic device were similar with those measured in the human intestine with difference of 0.96-fold, but it was different from those measured in the rat intestine with 8-fold. The difference in the in vivo permeability values between human and rat is caused by the difference of effective absorptive area of the perfused segment, permeation pathway of species, and lipid content in cellular membrane. Additionally, the diffusion coefficient and diffusion distance are also the causes for the permeability difference.[32,33] Some outlying values in the permeability correlation may be attributable to the differential effects of efflux or absorptive mechanisms among human, rat, and trapped Caco-2 cells.[23] In the case of high-permeability drugs with human P_{eff} greater than 8×10^{-4} cm/s, such as naproxen, and/or low-permeability drugs with human P_{eff} less than 4×10^{-4} cm/s, such as furosemide, the correlations were higher than for intermediate-permeability drugs with human P_{eff} between 5×10^{-4} and 7×10^{-4} cm/s, such as verapamil, antipyrine, and carbamazepine. As the intermediate-permeability drugs are affected by solubility, the permeability of drugs can vary with absorptive conditions, such as the solvent, reaction process, and fluid flow.[34] Note that P_{eff} on the microfluidic device showed a stronger correlation with that in the human intestine compared to that in the rat intestine.

In addition, we carried out a *t* test to check whether the measured permeability on our device is statistically meaningful

(24) Zakeri-Milani, P.; Valizadeh, H.; Azarmi, Y.; Barzegar-Jalali, M.; Tajerzadeh, H. *Daru* **2006**, *14*, 102–108.
(25) Venkatesh, G.; Ramanathan, S.; Mansor, S. M.; Nair, N. K.; Sattar, M. A.; Croft, S.; Navaratnam, V. *J. Pharm. Biomed. Anal.* **2007**, *43*, 1546–1551.
(26) Hempenius, J.; Wieling, J.; Brakenhoff, J. P. G.; Maris, F. A.; Jonkman, J. H. G. *J. Chromatogr.* **1998**, *714*, 361–368.
(27) Palmgren, J. J.; Monkkonenb, J.; Jukkola, E.; Niva, S.; Auriola, S. *Eur. J. Pharm. Biopharm.* **2004**, *57*, 319–328.
(28) Irvine, J. D.; Takahashi, L.; Lockhart, K.; Cheong, J.; Tolan, J. W.; Selick, H. E.; Grove, J. R. *J. Pharm. Sci.* **1999**, *88* (1), 28–33.
(29) Pade, V.; Stavchansky, S. *J. Pharm. Sci.* **1998**, *87*, 1604–1607.
(30) Flaten, G. E.; Dhanikula, A. B.; Luthman, K.; Brandl, M. *Eur. J. Pharm. Sci* **2006**, *27*, 80–90.
(31) Augustijns, P.; Mols, R. *J. Pharm. Biomed. Anal.* **2004**, *34*, 971–978.
(32) Fagerholm, U.; Johansson, M.; Lennernäs, H. *Pharm. Res.* **1996**, *13* (9), 1336–1342.
(33) Morimoto, Y.; Hatanaka, T.; Sugibayashi, K.; Omiya, H. *J. Pharm. Pharmacol.* **1996**, *44* (8), 634–639.
(34) Amidon, G. L.; Lennernäs, H.; Shah, V. P.; Crison, J. R. *Pharm. Res.* **1995**, *12*, 413–420.
(35) Kasim, N. A.; Whitehouse, M.; Ramachandran, C.; Bermejo, M.; Lennernäs, H.; Hussain, A. S.; Junginger, H. E.; Stavchansky, S. A.; Midha, K. K.; Shah, V. P.; Amidon, G. L. *Mol. Pharm.* **2004**, *1*, 85–96.
(36) Lennernäs, H. *J. Pharm. Sci.* **1998**, *87*, 403–410.

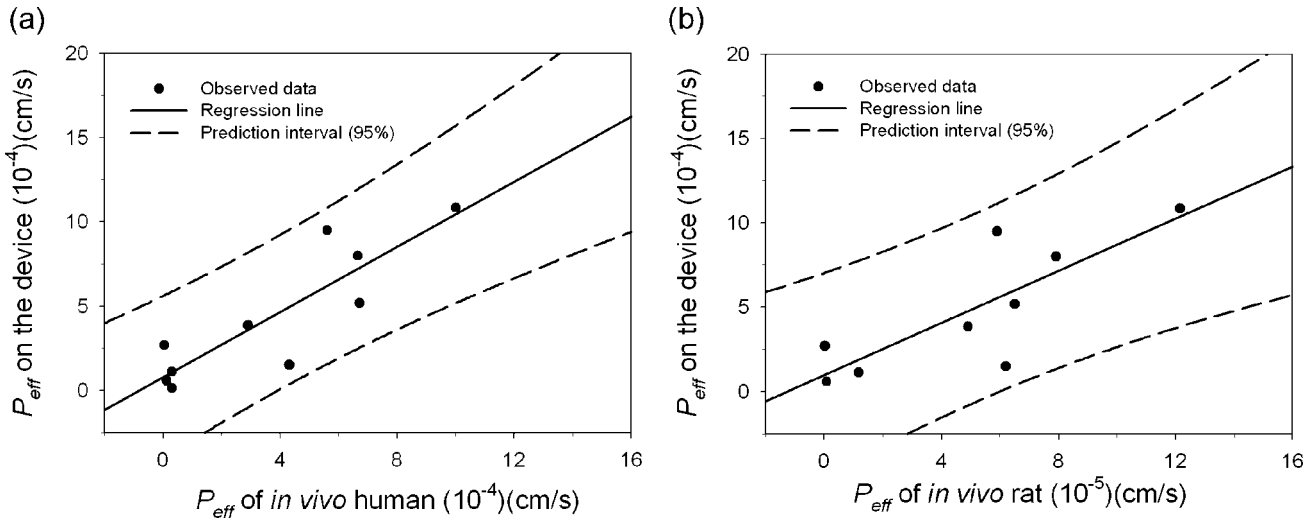

Figure 5. Comparison of drug permeability measured on the microfluidic device vs the human and rat intestine. (a) Comparison of drug permeability assayed on the microfluidic device vs the human intestine. (b) Comparison of permeability measured on the microfluidic device vs the rat intestine.

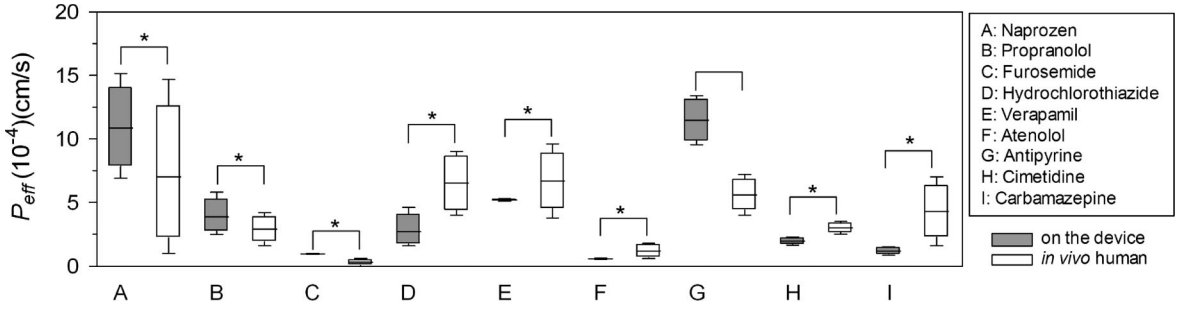

Figure 6. Comparison of the effective permeability (P_{eff}) on the device and in vivo human. * p values from t test are larger than 0.05 ($n \geq 3$).

or not, compared to that of in vivo data. As shown in Figure 6, most drugs, including naproxen, propranolol, and furosemide, had a high p value ($p > 0.4$), and only a few drug such as antipyrine had a low p value less than 0.05. Their measured permeabilities are not the same as those in vivo human intestine, but as shown in Figure 5, they are still highly correlated with in vivo permeabilities. Therefore, our device is able to produce a significant value compared to the permeability values of in vivo data and to measure in vivo permeability.

Correlation with F_a and P_{eff}. We compared the fraction of the dose absorbed in the human intestine (F_a) with the P_{eff} measured on the microfluidic device because F_a represents the actual drug absorption in the human intestine. As shown in Figure 7, the permeability measured on the microfluidic device and F_a were significantly correlated:[1]

$$F_a \text{ (human intestine)} = 1 - e^{-1.0634 P_{eff} \text{ (device)}} \quad (5)$$

The obtained P_{eff} on the microfluidic device showed a high correlation ($R^2 = 0.9641$) with human F_a.[1,30] In the case of low-permeability drugs with F_a below 70%, the P_{eff} on the microfluidic device was inconsistent with F_a because of differences in the effective absorptive area and mechanism of absorption. In highly permeable drugs of more than 90% F_a, the P_{eff} values were closely correlated with F_a because such drugs can be rapidly absorbed and saturated to a steady state over the differences in the absorption mechanism between the human intestine and trapped cells on the microfluidic device. Similar to the strong correlation between in vivo human P_{eff} and P_{eff} on the microfluidic device, the strong correlation between F_a and P_{eff} on the microfluidic device indicated that this device can be used to replace conventional permeability assays by predicting human permeability more precisely.

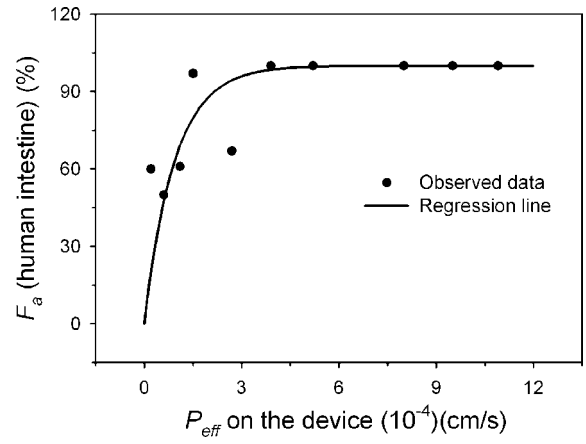

Figure 7. Plot of the effective permeability (P_{eff}) on the device vs the fraction of dose absorbed in the human intestine (F_a).

CONCLUSIONS

We developed an efficient microfluidic device for performing permeability assays. The microfluidic structure and its experimental conditions were optimized by mathematical simulations, and the results were experimentally validated. As trapped cells were viable without cell lysis on the microhole array, FITC−dextran was used to verify the absorption of drugs through trapped cells; the intensity of FITC−dextran was saturated after 2 h. On the basis of these experiments, we performed the permeability assay with 10 drugs. The trapped cells were viable after drug absorption and the permeability coefficient between human in vivo and P_{eff} on the microfluidic device was related significantly. These results indicated that our drug permeability assay device will be useful in predicting the actual human permeability values of drugs. In addition, our permeability assay system reduces the assay time as no cell culture on the microfluidic device is required and no complex structure, such as cellular membrane, is needed. With the use of trapped cells mimicking the intestinal epithelial cells, the integrated system including toxicity assay can be used as a valuable tool in drug discovery, and its applicability will be extended to include ADME/Tox drug properties.[37−40] However, since single cells are trapped in each microhole for a short period, no tight cell junction is formed even if Caco-2 cells mimic in vivo environments. Consequently, the condition on our device is not exactly the same as that of in vivo, and our device could not measure the drug absorption through the cell junctions. However, a total of 95% drugs are transported passively or actively in aid of transport proteins and only 5% drugs are transported by paracellular pathways through the cell junctions. In this sense, our strategy can be applied to the drugs absorbed passively or actively, which covers 95% of drugs available.

(37) Waterbeemd, H.; Gifford, E. *Nat. Rev. Drug Discovery* **2003**, *2*, 192–204.
(38) Yu, H.; Adedoyin, A. *Drug Discovey Today* **2003**, *8*, 852–861.
(39) Li, A. P. *Drug Discovery Today* **2001**, *6*, 357−366.
(40) Gómez-Hens, A.; Aguilar-Caballos, M. P. *Trends Anal. Chem.* **2007**, *26*, 171–182.

ACKNOWLEDGMENT

This work was supported by the Korea Science and Engineering Foundation (KOSEF) NRL Program Grant (R0A-2008-000-20109-0) funded by the Korea government (MEST) and by the Industrial Technology Development Program Grant (10017755) of the Korea government (MKE). The authors also thank the Chung Moon Soul Center for BioInformation and BioElectronics, KAIST.

SUPPORTING INFORMATION AVAILABLE

Additional information as noted in text. This material is available free of charge via the Internet at http://pubs.acs.org.

Received for review November 6, 2008. Accepted January 19, 2009.

AC802351W